Front. Eng. Manag. 2019, 6(1): 70–77
https://doi.org/10.1007/s42524-019-0005-8

RESEARCH ARTICLE

Tingting DU, Wenjing DU

Characteristics of flow and heat transfer of shell-and-tube heat exchangers with overlapped helical baffles

Abstract The characteristics of flow and heat transfer of shell-and-tube heat exchangers with overlapped helical baffles (STHXsHB) were illustrated through a theoretical analysis and numerical simulation. The ideal helical flow model was constructed to demonstrate parts of the flow characteristics of the STHXsHB, providing theoretical evidence of short-circuit and back flows in a triangular zone. The numerical simulation was adopted to describe the characteristics of helical, leakage, and bypass streams. In a fully developed section, the distribution of velocity and wall heat transfer coefficient has a similar trend, which presents the effect of leakage and bypass streams. The short-circuit flow accelerates the axial velocity of the flow through the triangular zone. Moreover, the back flow enhances the local heat transfer and causes the ascent of flow resistance. This study shows the detailed features of helical flow in STHXsHB, which can inspire a reasonable optimization on the shell-side structure.

Keywords heat exchanger, overlapped helical baffle, triangular zone, helical flow

1 Introduction

A shell-and-tube heat exchanger is the most widely used heat transfer equipment in industries making up to 37% of heat exchangers (Pletcher and Andrews, 1994). The equipment is substantially applied in relatively poor working conditions; thus, fouling, which can reduce the operational lifetime and can ultimately result in the failure of the exchanger, has become the primary problem. The capital loss caused by the fouling of heat exchangers accounted for 0.25%–0.3% of the gross national products in most industrial countries (Steinhagen et al., 1993). Thus, fouling prevention must be significantly considered in the design of shell-and-tube heat exchangers.

Master et al. (2003) used a hydrodynamic mechanism and reported that fouling in the shell-and-tube heat exchanger is mainly induced by uneven velocity flow, backflow, and eddies for the improperly designed structure in the shell side. To solve this problem, Lutcha and Nemcansky (1990) proposed a helical flow alternative to the zigzag flow in the exchanger with segmental baffles. The baffles in this alternative were angled to the axis of the heat exchanger and were overlapped at the outer periphery of the shell, as shown in Fig. 1. As the flow in the pseudo-helical flow passage approaches the plug flow, shell-and-tube heat exchangers with overlapped helical baffles (STHXsHB) can effectively reduce flow resistance, weaken the vibration of the tube bundle, prevent shell-side fouling, and markedly increase heat transfer coefficient per pressure drop. However, the leakage stream in a

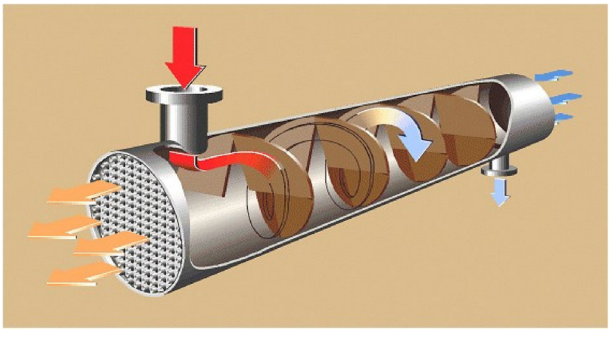

Fig. 1 Principle of the heat exchanger with helical baffles (Lutcha and Nemcansky, 1990)

Received March 30, 2018; accepted June 5, 2018

Tingting DU (✉), Wenjing DU
School of Energy and Power Engineering, Shandong University, Jinan 250061, China
E-mail: dutingting@sdu.edu.cn

This work was supported by the National Basic Research Program of China (Grant No. 2013CB228305) and the International Clean Energy Talent Program (China Scholarship Council [2017]5047, [2018]5023).

triangular zone formed by the adjacent baffles can produce short-circuit effect and back flow, which pronouncedly influence the plug-like flow situation (Du et al., 2013). In prior studies, the triangular zone has been taken as the major optimized object prevailingly by blocking the leakage through this zone to increase the overall heat transfer coefficient (Cao et al., 2012; Wen et al., 2015; Dong et al., 2016). Although these optimizations can enhance heat transfer to an extent, the pressure drop increases accordingly, resulting in the decrease in comprehensive performance (Wang et al., 2001). Therefore, further research on the characteristics of leakage stream through the triangular zone is necessary to achieve a desirable design.

At present, most investigations have focused on the overall characteristics of heat transfer and flow in the shell side of the STHXsHB. The trends in the characteristics of helix angle associated with the triangular zone have been presented by numerical simulations and experiments (Stehlik et al., 1994; Kral te al, 1996; Wang, 2002; Jafari et al., 2008), however, few studies have featured the leakage manner and depicted local characteristics in detail. The present work aims to discern the mechanism of the leakage stream through the triangular zone by a theoretical analysis and numerical simulation and offer evidence for future optimizations on heat transfer enhancement without dramatic increases in pressure drop.

2 Theoretical analysis on the shell-side flow

As the flow in the shell side of the STHXsHB approaches the plug flow, an ideal helical flow model is built when it is supposed as a steady laminar flow, and the leakage and bypass streams are ignored. On the basis of these hypotheses, the ideal helical flow can be considered the combination of Hagen–Poiseuille and Couette flows. Moreover, if the curve of motion for any infinite element in the domain is presumed as the constant-pitch helix, then the vortex line and streamline can coincide in the ideal helical flow field. The mathematical expressions describing the mass, momentum, and energy conservation are represented in the cylindrical coordinate (r, θ, z) as (Ji, 2011)

Continuity:

$$\frac{\partial\rho}{\partial t}+\frac{1}{r}\left[\frac{\partial(r\rho v_r)}{\partial r}+\frac{\partial(\rho v_\theta)}{\partial\theta}+\frac{\partial(r\rho v_z)}{\partial z}\right]=0; \quad (1)$$

Momentum:

$$\rho\left(\frac{Dv_r}{Dt}+\frac{{v_\theta}^2}{r}\right)$$

$$=\rho f_r+\frac{1}{r}\left[\frac{\partial(rp_{rr})}{\partial r}+\frac{\partial(p_{\theta r})}{\partial\theta}+\frac{\partial(rp_{zr})}{\partial z}-p_{\theta\theta}\right], \quad (2)$$

$$\rho\left(\frac{Dv_\theta}{Dt}+\frac{v_\theta v_r}{r}\right)$$

$$=\rho f_\theta+\frac{1}{r}\left[\frac{\partial(rp_{r\theta})}{\partial r}+\frac{\partial(p_{\theta\theta})}{\partial\theta}+\frac{\partial(rp_{z\theta})}{\partial z}+p_{r\theta}\right], \quad (3)$$

$$\rho\frac{Dv_z}{Dt}=\rho f_z+\frac{1}{r}\left[\frac{\partial(rp_{rz})}{\partial r}+\frac{\partial(p_{\theta z})}{\partial\theta}+\frac{\partial(rp_{zz})}{\partial z}\right]; \quad (4)$$

Energy:

$$\rho c_v\frac{DT}{Dt}=\rho q+\frac{1}{r}\left[\frac{\partial}{\partial r}\left(rk\frac{\partial T}{\partial r}\right)+\frac{\partial}{\partial\theta}\left(\frac{k\partial T}{r\,\partial\theta}\right)\right.$$

$$\left.+\frac{\partial}{\partial z}\left(rk\frac{\partial T}{\partial z}\right)\right]-p\mathrm{div}\mathbf{V}+\Phi, \quad (5)$$

where the material derivative is

$$\frac{D}{Dt}=\frac{\partial}{\partial t}+v_r\frac{\partial}{\partial r}+\frac{v_\theta}{r}\frac{\partial}{\partial\theta}+v_z\frac{\partial}{\partial z}. \quad (6)$$

Generally, the fluid is incompressible and viscous, and the density and the viscosity are constant. Thus, the divergence of flow velocity is

$$\nabla\cdot\mathbf{V}=0. \quad (7)$$

Assuming that the helical baffle is continuous, the equation to describe the helical surface is

$$\begin{cases}x=r\cos(\omega t)=r\cos\theta\\ y=r\sin(\omega t)=r\sin\theta\\ z=H_p\theta/2\pi=\theta r\mathrm{tg}\beta\end{cases}$$

$$\left(0\leqslant r\leqslant\frac{D_s}{2},0\leqslant\theta\leqslant2\pi,0\leqslant z\leqslant H_p\right), \quad (8)$$

where D_s is the inner diameter of the exchanger; H_p is the helical pitch for a period; and β is the helix angle, which is defined as the inclination angle of the baffle to the axil of the exchanger.

In an ideal helical flow, the velocity vectors in radial, axial, and tangential directions satisfy

$$v_r=0, \quad (9)$$

$$\frac{v_z}{v_\theta}=\frac{D_s}{2r}\mathrm{tg}\beta. \quad (10)$$

In the fully developed flow region, the boundary conditions are

$$v_r\Big|r=\frac{D_s}{2}=v_\theta\Big|r=\frac{D_s}{2}=v_Z\Big|r=\frac{D_s}{2}=0, \quad (11)$$

$$v_r\Big|Z=\theta\frac{D_s}{2}\mathrm{tg}\beta=v_\theta\Big|Z=\theta\frac{D_s}{2}\mathrm{tg}\beta=v_Z\Big|$$

$$Z = \theta\frac{D_s}{2}\mathrm{tg}\beta = 0, \tag{12}$$

$$\left.\begin{aligned} v_r|r = r_0,\theta = \theta_0,z = 0 = v_r|r = r_0,\theta = \theta_0,z = \pi D_s\mathrm{tg}\beta \\ v_\theta|r = r_0,\theta = \theta_0,z = 0 = v_\theta|r = r_0,\theta = \theta_0,z = \pi D_s\mathrm{tg}\beta \\ v_z|r = r_0,\theta = \theta_0,z = 0 = v_z|r = r_0,\theta = \theta_0,z = \pi D_s\mathrm{tg}\beta \end{aligned}\right\}. \tag{13}$$

Subsequently, the basic equations can be simplified as Continuity:

$$\frac{1}{r}\frac{\partial v_\theta}{\partial\theta} + \frac{\partial v_z}{\partial z} = 0; \tag{14}$$

Momentum:

$$\rho\frac{{v_\theta}^2}{r} = \frac{\partial p}{\partial r} + \mu\left(\frac{2}{r^2}\frac{\partial v_\theta}{\partial\theta}\right), \tag{15}$$

$$\rho\left(\frac{v_\theta}{r}\frac{\partial v_\theta}{\partial\theta} + v_z\frac{\partial v_\theta}{\partial z}\right) = -\frac{1}{r}\frac{\partial p}{\partial\theta} + \mu\left(\nabla^2 v_\theta - \frac{v_\theta}{r^2}\right), \tag{16}$$

$$\rho\left(\frac{v_\theta}{r}\frac{\partial v_z}{\partial r} + v_z\frac{\partial v_z}{\partial z}\right) = -\frac{\partial p}{\partial z} + \mu\nabla^2 v_z; \tag{17}$$

Energy:

$$\rho c_v\left(\frac{v_\theta}{r}\frac{\partial T}{\partial\theta} + v_z\frac{\partial T}{\partial z}\right) = \rho q + k\nabla^2 T + \Phi, \tag{18}$$

where ∇^2 is the Laplacian with the following expression in the cylindrical coordinate:

$$\nabla^2 = \frac{\partial^2}{\partial r^2} + \frac{1}{r}\frac{\partial}{\partial r} + \frac{1}{r^2}\frac{\partial^2}{\partial\theta^2} + \frac{\partial^2}{\partial z^2}. \tag{19}$$

In STHXsHB, a force induced by the baffle is imposed on the fluid. In terms of Hagen–Poiseuille law and the simplified equations of the ideal helical flow, the shear stresses on the upwind and back sides of the baffle have the same value but in the opposite direction. The equation of the shear stress is

$$\tau_H = \mu\frac{\partial v}{\partial\overline{n}}\Big|_H = \mu\left(\frac{1}{r}\frac{\partial v_\theta}{\partial\theta}\cos\beta + \frac{\partial v_z}{\partial z}\sin\beta\right)\Big|_H. \tag{20}$$

By taking Eq. (14) into Eq. (20), the friction resistance F_{fr} on the surface of the baffle yields

$$F_{\mathrm{fr}} = \sin\beta(\cos\beta - \sin\beta)\left(\mu\frac{\partial v_z}{\partial z}\Big|_{H+} - \mu\frac{\partial v_z}{\partial z}\Big|_{H-}\right), \tag{21}$$

where $H+$ and $H-$ represent the shear stress on the upwind and back sides of the baffle, respectively.

In addition, the pressure difference can be acquired by integration in one period, as shown as follows:

$$\Delta p\Big|_{z=\frac{\theta D_s\mathrm{tg}\beta}{2}} = \int_0^{2\pi}\frac{\partial p}{r\partial\theta}d\theta\Big|_{z=\frac{\theta D_s\mathrm{tg}\beta}{2}}. \tag{22}$$

Combining Eqs. (16) and (22) yield

$$\Delta p\Big|_{z=\frac{\theta D_s\mathrm{tg}\beta}{2}} = \int_0^{2\pi}\mu\left(\nabla^2 v_\theta - \frac{v_\theta}{r^2}\right)d\theta\Big|_{z=\frac{\theta D_s\mathrm{tg}\beta}{2}}. \tag{23}$$

Hence, the pressure resistance F_{pr} is

$$\begin{aligned} F_{\mathrm{pr}} &= \cos\beta\cdot\Delta p\Big|_{z=\frac{\theta D_s\mathrm{tg}\beta}{2}} \\ &= \cos\beta\int_0^{2\pi}\mu\left(\nabla^2 v_\theta - \frac{v_\theta}{r^2}\right)d\theta\Big|_{z=\frac{\theta D_s\mathrm{tg}\beta}{2}}. \end{aligned} \tag{24}$$

When r approaches 0 and β approaches $\pi/2$, the limit of F_{pr} is

$$\lim_{r\to 0} F_{\mathrm{pr}} = 0. \tag{25}$$

This finding indicates that pressure resistance can acquire the extreme value at the center of the cylinder. When F_{pr} approaches 0, the friction in the axial direction ($\partial v_z/\partial z$) and v_z increases steeply. The theoretical analysis demonstrates the characteristics of the helical flow and accounts for the mechanism of the short-circuit flow in the triangular zone and the flow acceleration in the axial direction.

3 Numerical simulation on the shell-side characteristics

The ideal helical flow model is established in the theoretical analysis; thus, a numerical simulation was adopted to present the actual characteristics of the STHXsHB, especially the feature of the leakage flow through the triangular zone, which can verify the feasibility of the mathematical model.

3.1 Geometrical model and parameters

The reasonable simplification for the geometry of the STHXsHB is necessary to obtain the robustness of conclusion and save time in calculation. In this numerical simulation, the assumptions are listed as follows.

(1) The wall thicknesses of the shell and the tube are ignored.

(2) Installations and reinforcement structures in the shell side are ignored.

(3) The baffle-to-shell leakage is ignored.

(4) The baffle-to-tube leakage is ignored.

The geometrical model is presented in Fig. 2, and the parameters are listed in Table 1.

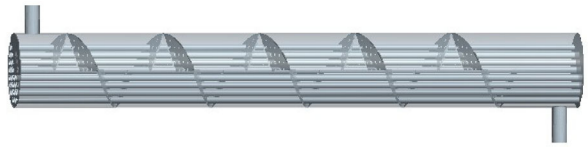

Fig. 2 Geometrical model of the STHXsHB

Table 1 Parameters of the STHXsHB

Item	Size/Quantity
Inner diameter of shell D_s (mm)	207
Inner diameter of inlet and outlet D_{in}, D_{out} (mm)	40
Outer diameter of tubes d_t (mm)	19
Tube length L_t (mm)	1600
Central distance of tubes t_p (mm)	24
Number of tubes N_t	55
Helix period n	5
Helix angle β (°)	25°
Tube layout	Regular triangular
Thickness of baffles s_b (mm)	3
Overlap size e (%)	0

3.2 Governing equations and boundary conditions

The general governing equation for the turbulent convective heat transfer is (Tao, 2001)

$$\mathrm{div}(\rho U\phi) = \mathrm{div}(\Gamma_\phi \mathrm{grad}\phi) + \mathrm{S}_\phi, \tag{26}$$

where the generalized variable ϕ can represent the velocity vector and temperature, among others. When the generalized diffusion coefficient Γ_ϕ and generalized source term S_ϕ have different values, Eq. (26) can accordingly express the continuity, momentum, and energy equations and the k-ε turbulence model.

The initial data and boundary conditions for the STHXsHB are set as follows. The inlet stream is water with constant physical properties and the temperature is specified as 313.15 K. The tube bundle remains the constant wall temperature specified as 353.15 K. The stream flows freely out of the exchanger. The surface of baffles and the inner wall of the shell are considered the thermal isolation. Moreover, the turbulent flow is steady, and buoyancy and gravity are ignored.

3.3 Grid independence and reliability verification of the numerical calculation

The grid system was established by ICEM15.0 on the 3D geometry created by Pro/Engineer 5.0. The computational domain was meshed with unstructured tetrahedron, hexahedron, and pyramid elements. Meshes were taken to refine and coarsen for three times on the basis of the gradient of adaptive variables, including temperature and pressure. The grid independence was tested with the results shown in Fig. 3, and the mesh with 9.8×10^6 grid numbers was adopted in consideration of the calculation time.

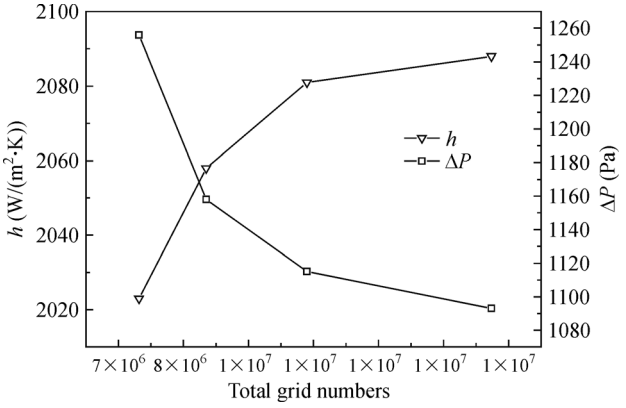

Fig. 3 Grid independence verification

The computational results were verified by the experimental results of the heat exchanger with helical baffles at a helix angle of 15° (Wang, 2001). As shown in Figs. 4 and 5, the deviations of pressure drop and heat transfer coefficient are 14.7%–21.5% and 9.0%–14.8%, respectively. The deviations mainly result from the model simplification, assumption, and ignorance of initial and boundary conditions, as well as the intrinsic error of the experiment. The numerical simulation is verified to be reliable as the range of deviation can be accepted in engineering applications.

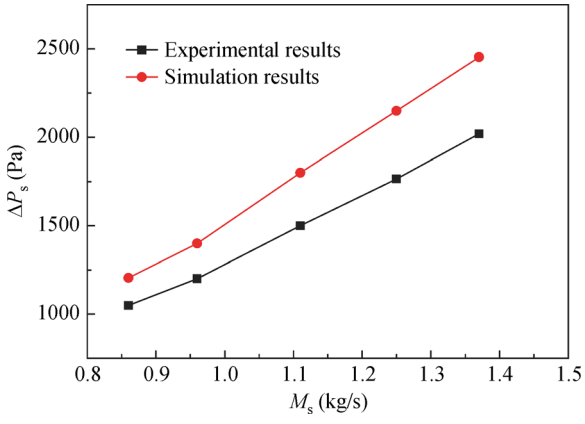

Fig. 4 Shell-side pressure drop comparison between the simulation and experimental results

The helical flow in the shell side is highly complex with a high strain rate; hence, RNG (Re-nomalization Group) k-ε turbulence model was adopted to obtain an accurate streamline with a large bent degree. High resolution was applied, and RMS was set to less than 1.0×10^{-5}.

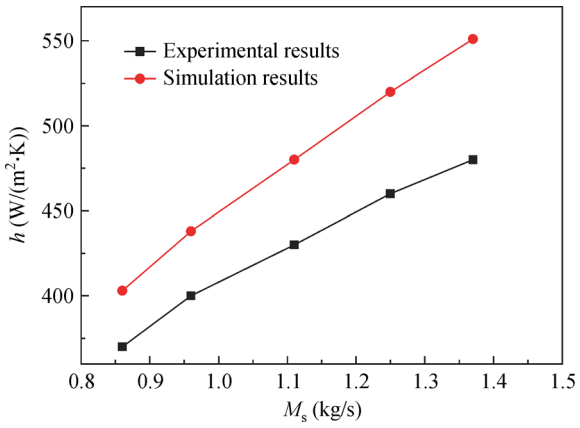

Fig. 5 Shell-side heat transfer coefficient comparison between the simulation and experimental results

4 Characteristics of flow and heat transfer

4.1 Characteristics of heat transfer in the axial direction

The average heat transfer coefficient in the shell side was read at intervals of 50 mm in the axial direction, with the beginning and ending at 100 mm away from the two opposite sides of the shell. The distribution of the heat transfer coefficient for the inlet mass flow rate at 4 kg/s and the helix angle at 25° is shown in Fig. 6. The curve of the coefficient depicts three sections. On the basis of the feature of the curve, the inner flow in the shell side of STHXs can be divided into three sections which are respectively named as the inlet section, the fully-developed section, and the outlet section. The inlet section is located approximately in the range of 0–400 mm. The heat transfer coefficient in this section is considerably larger than those in the other two sections due to the abrupt extension of the area. Similarly, in the outlet section, starting nearly at 1400 mm, the sudden shrinkage in area increases the turbulent flow and a relatively high coefficient is obtained. Comparatively, the curve, except in the inlet and outlet sections, slightly fluctuates and represents a periodical scheme, where the flow can be considered to have been fully developed. In this study, the performance of the STHXsHB is the focus of investigation.

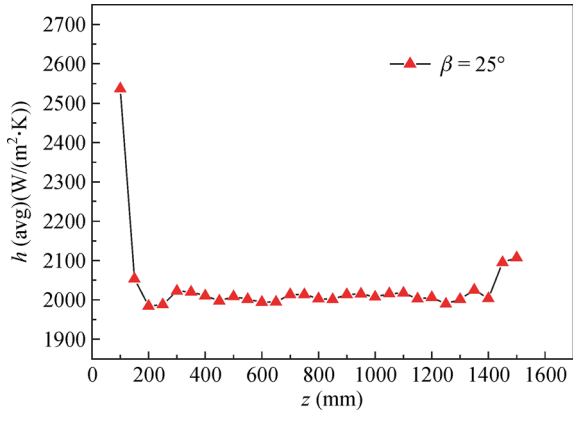

Fig. 6 Distribution of the average heat transfer coefficient in the axial direction ($\beta = 25°$, $M = 4$ kg/s)

4.2 Characteristics of heat transfer in the radial direction

One-quarter of the tube bundle was picked up for the local characteristic study in a fully developed period due to the symmetry of four-baffle arrangement, and each of the selected tubes was marked by capitals, as shown in Fig. 7. The average wall heat transfer coefficient of each tube is plotted versus the Reynolds number *Re* in Fig. 8. The coefficient increases as the *Re* increases and the radius decreases. According to the distribution condition, 17 tubes can be sorted out into three groups. The first group includes the tubes of E, A, B, P, I, and F, which are located

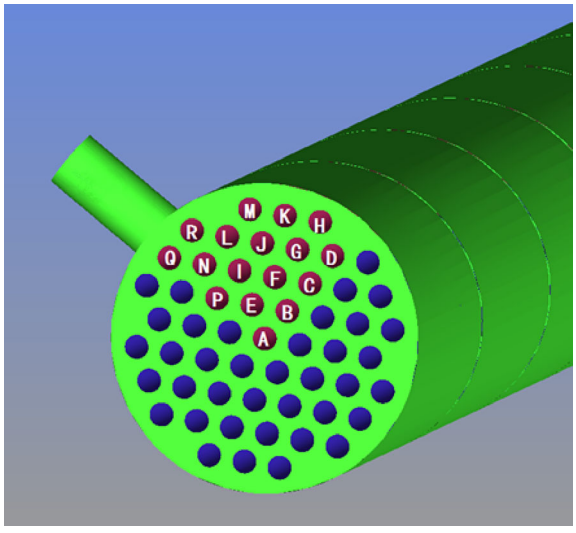

Fig. 7 Tube label

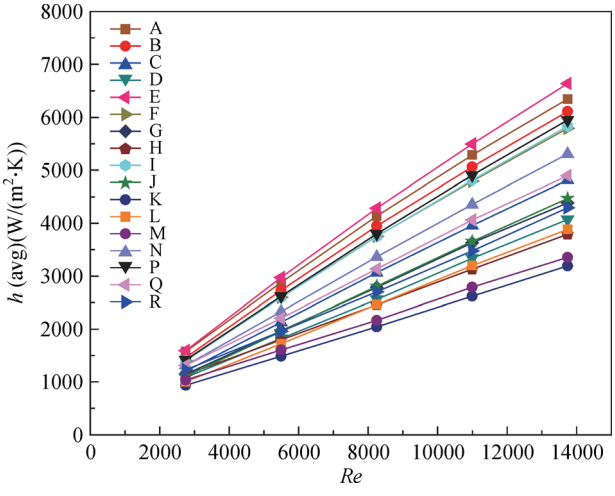

Fig. 8 Average wall heat transfer coefficient of each tube versus *Re* ($\beta = 25°$)

in the center of the shell. In this group, the triangular zone formed by two adjacent baffles, tips, and edges of the baffles greatly affects the turbulent flow and has a relatively high wall heat transfer coefficient. Another group with a relatively small coefficient was centralized in the tube-to-shell region where the low-turbulent bypass stream mostly influences the tubes of H, M, and K. The helical flow crossing over the tubes of C, D, G, J, L, N, R, and Q is not in high turbulence; hence, the coefficients around the tubes are not extremely large. Although the helical flow is expected to generate vortex and enhance heat transfer (Lutcha and Nemcansky, 1990), the coefficient of a pure helical flow is not as high as that of the leakage in the triangular zone where the leakage is usually blocked for the increase in pressure drop. However, the triangular zone is a significant structure that influences the characteristics of heat transfer, and the optimized design on it can realize the enhancement of the heat transfer and reduce the increase in flow resistance.

4.3 Characteristics of flow in the axial direction

The streamline in a fully developed period is depicted in Fig. 9, which represents the shell-side flow characteristics for a helix angle of 25°. The lines in the tube-to-shell region present the obviously regular helical curves, which depict the even flow field caused by the bypass stream. In addition, the stream guided by the baffles features the helical flow with minor curvature and similar velocity values compared with the bypass flow. The flow through the triangular zone is special for the acceleration in the velocity and backflow. The red line passing through the triangular zone demonstrates the phenomenon of the short-circuit flow. The irregular blue lines at the back side of the baffle displays the tremendous velocity decrease or even the backflow phenomenon due to the large pressure differences between the upwind side and back side of baffles illustrated by the theoretical analysis. The multi-stream integration in the triangular zone enhances the heat transfer and pressure drop, which can explain the high wall heat transfer coefficient for the tubes located near the zone.

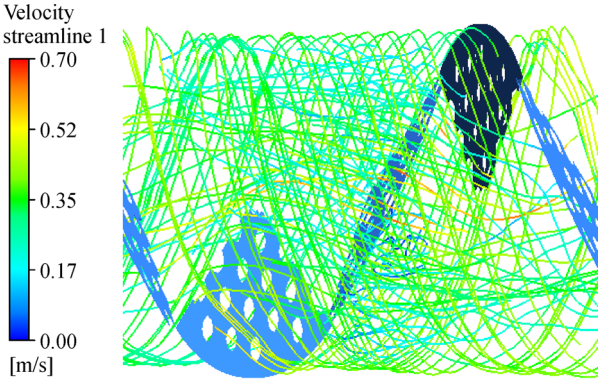

Fig. 9 Streamlines in the fully developed section ($\beta = 25°$, $M = 4$ kg/s)

4.4 Characteristics of the flow in the radial direction

The average velocity across the selected tubes with the same label is further depicted as the flow characteristics in the radial direction in Fig. 10. The feature of average velocity presents the similar trend with that of the wall heat transfer coefficient, which proves the close correlation between flow and heat transfer. The velocity vector and contour of the typical cross sections in different location of the shell side are shown in Fig. 11 and Fig. 12. The vector line density reflects the velocity value. Where there are more intensive lines, there is the larger velocity. Accordingly, the color in the contour is much redder. The global velocity field is obviously non-uniform, the velocity decreases with the increase of radius, which is the same with the trend of heat transfer coefficient distribution. In addition, the flow in the triangular leakage zone is more turbulent than that in other zones, which means more flow resistance is produced along the shell. Hence, the triangular zone is generally taken as the optimized object in order to reduce pressure drop.

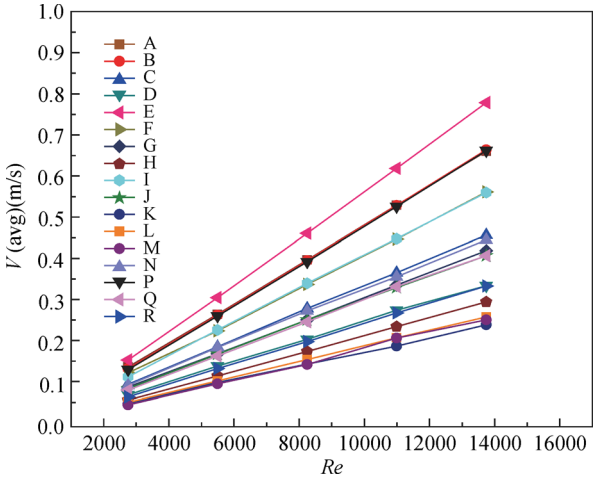

Fig. 10 Average velocity across each tube versus Re ($\beta = 25°$)

5 Conclusions

The characteristics of flow and heat transfer of STHXsHB are illustrated through a theoretical analysis and numerical simulation. The influence of the triangular leakage zone is represented on flow and heat transfer. The conclusions are drawn as follows.

(1) Parts of the flow characteristics of the STHXsHB can be described by the ideal helical flow model. The short-circuit and back flows, which probably appear in the triangular zone, can be demonstrated by the theoretical analysis.

(2) The flow field in the shell side of the STHXsHB is comprised of helical, leakage, and bypass streams. Flow

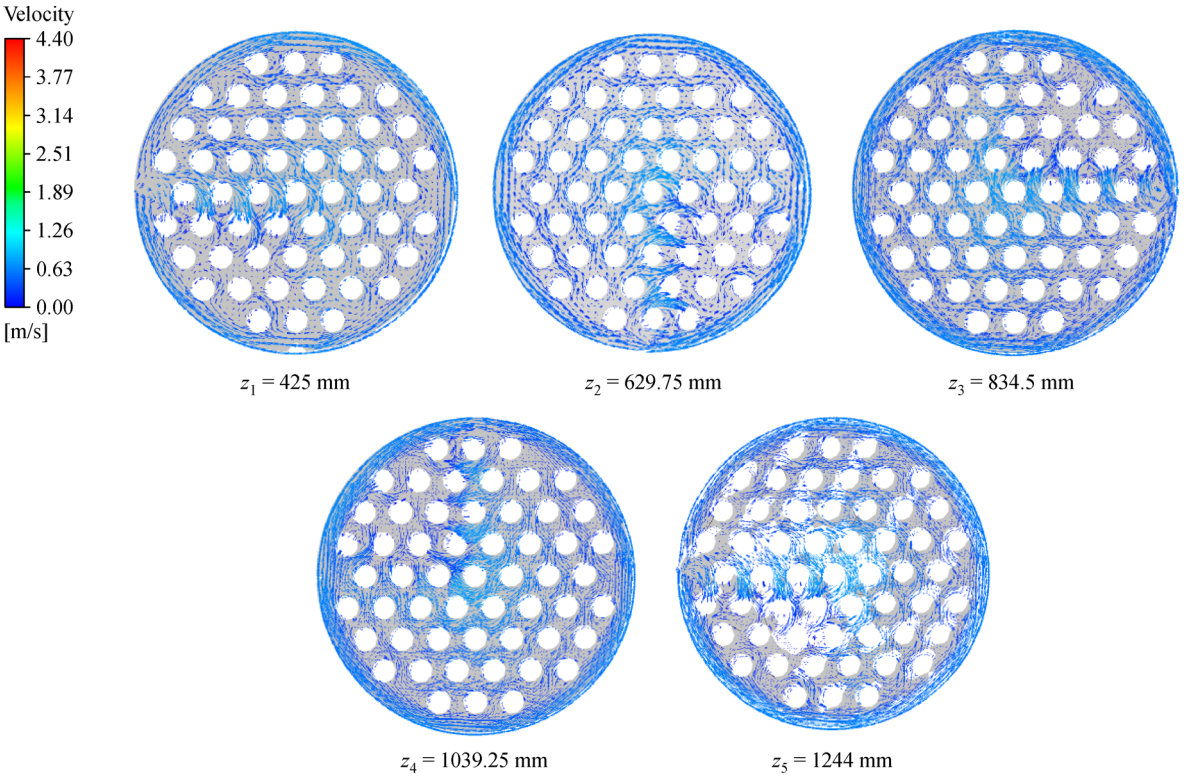

Fig. 11 Velocity vector in typical cross sections (β = 25°, V_s = 0.4 m/s)

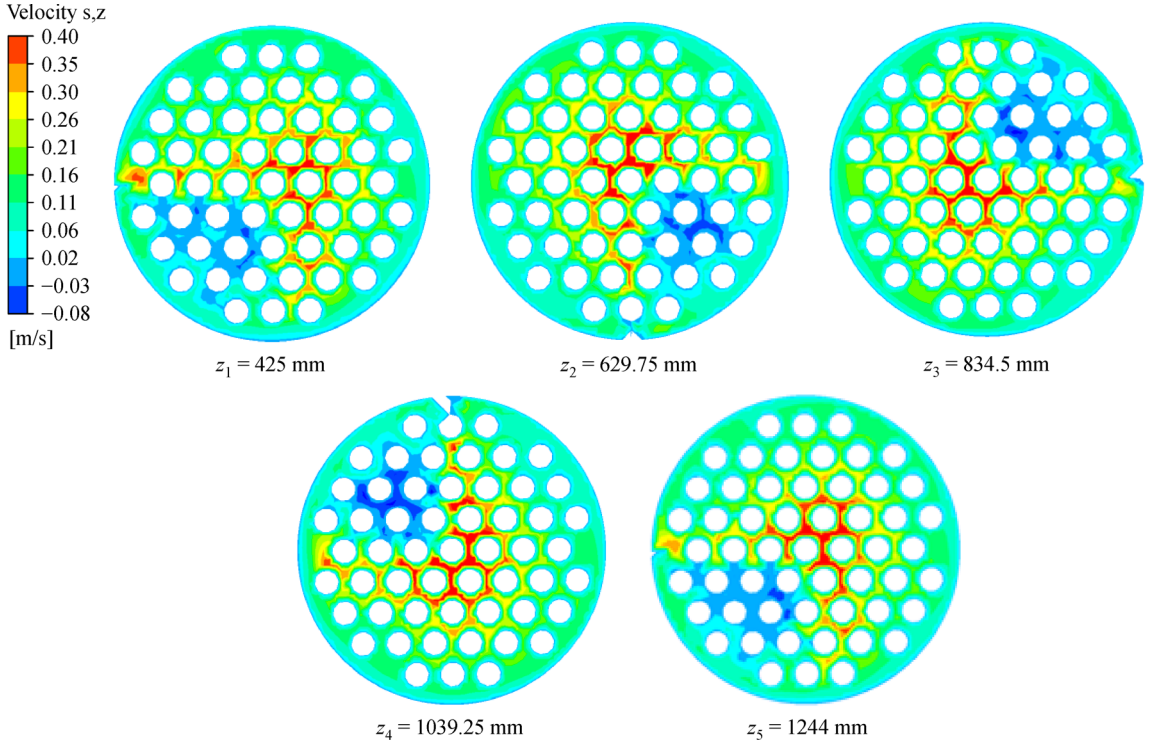

Fig. 12 Velocity contour in typical cross sections (β = 25°, V_s = 0.4 m/s)

Table 2 Nomenclatures

h	wall heat transfer coefficient (W/(m^2·K))	ϕ	General variable
M	mass flow rate (kg/s)	k	Turbulent kinetic energy (L^2T^{-2})
P	pressure (Pa)	ε	Turbulent kinetic energy dissipation rate (L^2T^{-3})
r	radius of shell (m)		Subscript
V	velocity (m/s)	avg	average value
Γ	generalized diffusion coefficient	t	tube side
S	generalized source term	s	shell side
β	helix angle (°)	z	axis of shell

characteristics indicate that the overall shell side can be divided into inlet, fully developed, and outlet sections. In the radial direction, the velocity of the fluid across the tube bundle generally increases with the decrease of radius. In the axial direction, the velocity of the leakage stream, which is affected by the triangular zone, is larger than those of the two other streams. Meanwhile, the back flow causes the increase of flow resistance, which results in a non-uniform velocity vector field.

(3) The heat transfer in the shell side is dramatically influenced by the flow, and the distribution of the wall heat transfer coefficient is mostly similar to the velocity distribution. The back flow in the triangular zone enhances the heat transfer; however, the heat transfer coefficient of the bypass flow is relatively low because its velocity is also low.

In summary, the triangluar leakage zone tremendously influences the characteristics of flow and heat transfer. Previous optimization works have emphasized on the reduction of flow resistance but have not referred to the effect of heat transfer enhancement. The overall heat transfer performance of STHXsHB is consistently inferior to that of shell-and-tube heat exhangers with segmental baffles with the same heat transfer areas. Therefore, the comparison of the respective amplification of heat transfer and pressure drop caused by the triangular zone is necessary in the future to determine the actual optimization design on the triangular zone and shell side.

References

Cao X, Du W J, Ji S H, Cheng L (2012). Influence of overlap size on shell-side performance of heat exchangers with helical baffles. Proceedings of the CSEE, 32(8): 78–84 (in Chinese)

Dong C, Li D, Zheng Y Q, Li G N, Suo Y G, Chen Y P (2016). An efficient and low resistant circumferential overlap trisection helical baffle heat exchanger with folded baffles. Energy Conversion and Management, 113: 143–152

Du W J, Wang H F, Cao X, Cheng L (2013). Heat transfer and fluid flow on shell-and-side of heat exchangers with novel sextant sector helical baffles. CIESC Journal, 64(9): 3123–3129 (in Chinese)

Jafari Nasr M R, Shafeghat A (2008). Fluid flow analysis and extension of rapid design algorithm for helical baffle heat exchangers. Applied Thermal Engineering, 28 (Compendex):1324–1332

Ji S H (2011). Mechanism analysis and performance study of flow and heat transfer in shell-side of shell-and-tube heat exchanger with helical baffles. Dissertation for the Doctoral Degree. Jinan: Shandong University (in Chinese)

Kral D, Stehlik P, Ploeg H J V D, Master B (1996). Helical baffles in shell-and-tube heat exchangers, Part I: Experimental verification. Heat Transfer Engineering, 17 (Compendex): 93–101

Lutcha J, Nemcansky J (1990). Performance improvement of tubular heat exchangers by helical baffles. Chemical Engineering Research & Design, 68(3): 263–270

Master B I, Chunangad K S (2003). Venkateswaran pushpanathan, fouling mitigation using helixchanger heat exchangers. In: Proceedings of 2003 ECI Conference on Heat Exchanger Fouling and Cleaning: Fundamentals and Applications. 43

Pletcher L S, Andrews M J (1994). Technical/market assessment of heat exchanger technology for users of natural gas. GRI Report GRI-94/0248

Stehlik P, Nemcansky J, Kral D, Swanson L W (1994). Comparison of correction factors for shell-and-tube heat exchangers with segmental or helical baffles. Heat Transfer Engineering, 15(Compendex): 55–65

Steinhagen R, Müller-Steinhagen H, Maani K (1993). Problems and costs due to heat exchanger fouling in New Zealand industries. Heat Transfer Engineering, 14(1): 19–30

Tao W Q (2001). Numerical Heat Transfer. Xi'an: Xi'an Jiaotong University Press (in Chinese)

Wang L (2001). The experimental study of heat transfer and pressure drop for shell-and-tube heat exchangers with helical bafffles. Dissertation for the Doctoral Degree. Xi'an: Xi'an Jiaotong University (in Chinese)

Wang L, Luo L Q, Wang Q W, Zeng M, Tao W Q (2001). Effect of inserting block plants on pressure drop and heat transfer in shell-snd-tube heat exchangers with helical baffles. Journal of Engineering Thermophysics, 22(s): 173–177

Wang S L (2002). Hydrodynamic studies on heat exchangers with helical baffles. Heat Transfer Engineering, 23(3): 43–49

Wen J, Yang H, Wang S M, Xue Y L, Tong X (2015). Experimental investigation on performance comparison for shell-and-tube heat exchangers with different baffles. International Journal of Heat and Mass Transfer, 84: 990–997